ECCOMAS Congress 2016
VII European Congress on Computational Methods in Applied Sciences and Engineering
M. Papadrakakis, V. Papadopoulos, G. Stefanou, V. Plevris (eds.)
Crete Island, Greece, 5–10 June 2016

TRANSITION FROM 2D CONTINUOUS ADJOINT LEVEL SET TOPOLOGY TO SHAPE OPTIMIZATION

J.R.L. Koch[1], **E.M. Papoutsis-Kiachagias**[1], **and K.C. Giannakoglou**[1]

[1]National Technical University of Athens (NTUA),
School of Mech. Eng., Parallel CFD & Optimization Unit
Athens, Greece
e-mail: kochjamesr@gmail.com, vaggelisp@gmail.com, kgianna@central.ntua.gr

Keywords: Adjoint-Based Optimization, Constrained Topology Optimization, Shape Optimization, Level Set Method, Topology to Shape Transition

Abstract. *The processes of topology and shape optimization are well known methods in the field of fluid mechanics. Although successful in their own rights, it is conceivable that the two methods will find choicest solutions in tandem: i.e. if shape optimization were able to improve a topological solution. Conjoining the two methods in this manner is not straightforward, however, since there is no existing process to connect one to the other. Toward this goal, a novel transitional process is proposed to process level set topology solutions obtained using the continuous adjoint method such that a shape optimization loop using the continuous adjoint can be initialized, run and ultimately produce a refined, parameterized solution. First, the topology optimization process is enhanced using the level set method to both maintain an explicit description of the interface between the solid and fluid topological domains and prevent the formation of fluid or solid islands which would not be viable for manufacturing. The interface is then fitted with Non-Uniform Rational B-Splines (NURBS) through application of sensitivities garnered from the solution of an auxiliary optimization problem which aims at reducing the difference between the signed distance fields generated about each NURBS curve and its corresponding interface section. A body-fitted mesh is generated for the geometry defined by the fitted NURBS, allowing a shape optimization loop to be initiated. The parameterized result of the topology to shape transition process will be compared to that of shape optimization in two 2D cases with internal, incompressible fluid flows.*

This research was funded by the People Programme (ITN Marie Curie Actions) of the European Union's H2020 Framework Programme (MSCA-ITN-2014-ETN) under REA Grant Agreement no. 642959 (IODA project). The first author is an IODA Early Stage Researcher.

1 INTRODUCTION

Topology optimization (TopO) was first proposed in [1] for the design of structural mechanics and was expanded to the field of fluid mechanics through the introduction of a blockage term (β) into the Stokes [2, 3] and laminar [4] flow equations which is treated as a design variable per grid cell and varied to minimize an objective function. On the other hand, shape optimization (ShpO) was initially introduced as shape control technique to reduce an objective function, [5], and is expanded to fluid mechanics using boundary mesh displacement to alter the original boundary shape of the case and, thus, its flow solution.

Both the TopO and ShpO processes require the ability to affect the current solution of a problem through design variable alteration in order to decrease (increase) the provided objective function(s). To this end, the adjoint method is employed to supply objective function sensitivities, effectively telling the design variable set in which way they should be altered. Continuous adjoint has been extensively developed for both ShpO and TopO for laminar and turbulent flows, [5, 6, 7, 8, 9], and is applied for the TopO and ShpO processes used in this work.

While TopO is commonly used in fluid mechanics to develop optimal flow paths between prescribed inlets and outlets according to the objective function(s) defined by the designer, ShpO is only capable of altering known boundaries of a geometry in order to obtain an optimal solution, but uses far fewer design variables (i.e., the boundary nodal or control point coordinates instead of an internal field) to do so. Ideally, a solution found using TopO could be used to begin a ShpO process which would produce a parameterized, manufacturable CAD model. However, solutions of TopO do not, on their own, contain the surface information required for ShpO to initialize; information which would be available if a fluid-solid interface (FSI) were explicitly defined by the TopO solution. Furthermore, TopO solutions found can also suffer from island formation and the development of grey-zones in which the FSI is ambiguous.

To address these issues, a process which conjoins the theories of both the continuous adjoint topology and level set (LS) optimization methods for incompressible viscous fluid simulations is devised and hereon associated with the term 'TopO'. The LS method is a conceptual framework, first proposed in [10], which maps moving interfaces through the introduction of a LS field (LSF) that corresponds to a signed-distance field. Integration of the LS method into TopO is achieved by making β a function of the LSF: the domain is modeled as solidified where the LSF is negative and fluidized when positive, making the zero-value contour of the LSF the FSI by definition. FSI progression toward an optimal solution occurs via adjoint sensitivity convection through alteration of cell-center LSF values and subsequent application of an accurate, fast-marching reinitialization algorithm.

The TopO-to-ShpO transition process begins by subdividing the FSI from TopO such that each division pertains to paired inlet-outlet connections. These FSI segments are used to initialize new individual LSFs which act as target solutions to a field-matching algorithm which tries to iteratively fit a NURBS curve to each segment. This is done by building a narrow band (NB) LSF about each NURBS curve, comparing it to the target LSF and, then, generating sensitivities for moving each NURBS control point (CP) based on their difference. A body-fitted mesh is generated from this NURBS fitting and is used to initialize an adjoint-driven ShpO process, which in turn generates a parameterized solution. This paper will apply the proposed method for conjoining the TopO and ShpO processes to two 2D test cases with the goal of minimizing total pressure losses in ducted flow using volumetric constraints. Both the cases and the in-house code pertaining to the coupling process are implemented within OpenFOAM2.2.1 [11].

2 TOPOLOGY OPTIMIZATION

2.1 Flow Equations

In this paper, the modeled fluid flow is governed by the steady-state Navier-Stokes equations for incompressible, laminar flows. The blockage formulation of TopO requires the addition of a term which contains a function of the blockage variable $(0 \leq \beta \leq 1)$ into the momentum equation (eq. 1b). If $f(\beta)$ becomes comparatively large, the added term becomes dominant, forcing the velocity toward zero and effectively rendering the domain solid. Conversely, if this term is comparatively small, the velocity is uninhibited and the domain remains fluid. The flow equations are

$$R_p = -\frac{\partial v_j}{\partial x_j} = 0 \tag{1a}$$

$$R_{v_i} = v_j \frac{\partial v_i}{\partial x_j} + \frac{\partial p}{\partial x_i} - \frac{\partial}{\partial x_j}\left[\nu\left(\frac{\partial v_i}{\partial x_j} + \frac{\partial v_j}{\partial x_i}\right)\right] + \underbrace{f(\beta)v_i}_{Blockage\ Term} = 0 \tag{1b}$$

where $f(\beta) = \beta\beta_{MAX}$ and β_{MAX} is a large and positive user-defined value. The usual primal boundary conditions associated with internal aerodynamics–constant inlet velocity, constant outlet pressure and no-slip condition along the wall–are imposed for all cases.

2.2 Adjoint Equations, Boundary Conditions and Sensitivities

In order to properly discuss the formulation of the adjoint equations, the basic TopO optimization problem must be examined. In this paper, the objective function to be minimized is that of the volume-averaged total pressure losses between the inlet(s), S_I, and outlet(s), S_O,

$$F = -\int_{S_I}\left(p + \frac{1}{2}v_k^2\right)v_i n_i dS - \int_{S_O}\left(p + \frac{1}{2}v_k^2\right)v_i n_i dS \tag{2}$$

where n_i are the components of the outward normal vector. To account for the possible inclusion of a constraint C into the TopO process, the objective function F to be minimized is re-defined as the Lagrangian objective function L according to the Augmented Lagrange Multiplier (ALM) method [12]. Constraints are discussed in Section 2.4. The optimization problem and corresponding Lagrangian function are defined as

$$\begin{aligned} &\min(F)\ ,\ \text{subject to}\ \ c = 0 \\ &L = F - \lambda c + wc^2 \end{aligned} \tag{3}$$

where c and λ are the constraint function and Lagrangian multiplier, respectively, and w is a dynamically changing weighting scalar [12]. If the constraint is not imposed $L \equiv F$. The Lagrangian function to be minimized is further augmented by the flow equation residuals as follows

$$L_{aug} = L + \int_\Omega q R_p d\Omega + \int_\Omega u_i R_{v_i} d\Omega \tag{4}$$

in which q and u_i are the adjoint pressure and velocity components, respectively. After lengthy derivation, [13], the variation of eq. 4 with respect to (w.r.t.) the design variable(s) β becomes

$$\begin{aligned} \frac{\delta L_{aug}}{\delta \beta_m} = &\int_\Omega R_q \frac{\partial p}{\partial \beta_m} d\Omega \ + \int_\Omega R_{u_i}\frac{\partial v_i}{\partial \beta_m} d\Omega \ + \int_\Omega v_i u_i \frac{\partial f(\beta)}{\partial \beta_m} d\Omega \\ &+ \int_S \mathcal{BC}_1 \frac{\partial p}{\partial \beta_m} dS + \int_S \mathcal{BC}_{2,i}\frac{\partial v_i}{\partial \beta_m} dS - \int_S \frac{\partial}{\partial \beta_m}\left[\nu\left(\frac{\partial v_i}{\partial x_j} + \frac{\partial v_j}{\partial x_i}\right)\right] u_i n_j dS \end{aligned} \tag{5}$$

where m is the cell index and S is the boundary of the computational domain Ω. The R and BC terms in eq. (5) will become the adjoint field equations and boundary conditions, respectively, and are derived through eliminating all terms with field integrals containing partial derivative(s) dependent on the β design variable(s) by setting their multipliers, or, in the case of the BC terms, portions of their multipliers, against zero. It should be noted that these partial derivatives are technically total derivatives: $\delta \equiv \partial$ for TopO since the computational grid remains unchanged when a design variable is changed [13].

The adjoint continuity and momentum field equations are defined as

$$R_q = \frac{\partial u_j}{\partial x_j} = 0 \tag{6a}$$

$$R_{u_i} = -v_j \left(\frac{\partial u_i}{\partial x_j} + \frac{\partial u_j}{\partial x_i} \right) + \frac{\partial q}{\partial x_i} - \frac{\partial}{\partial x_j} \left[\nu \left(\frac{\partial u_i}{\partial x_j} + \frac{\partial u_j}{\partial x_i} \right) \right] = 0 \tag{6b}$$

with appropriate boundary conditions derived from $\mathcal{BC}_1$ and $\mathcal{BC}_2$ (see [13]). After satisfaction of the field equations and their boundary conditions, the remaining terms of eq. 5 define the sensitivity derivatives of L_{aug} (here-on referred to as simply L) for laminar flows w.r.t. the blockage design variable(s)

$$\frac{\delta L}{\delta \beta_m} = \int_\Omega v_i u_i \frac{\partial f(\beta)}{\partial \beta_m} d\Omega = v_i^m u_i^m \Omega^m \beta_{MAX} \tag{7}$$

where Ω^m is the volume of the m-th grid cell.

2.3 Level Set Topology Formulation

Use of the blockage formulation of TopO creates two dilemmas w.r.t. the process of transitioning to ShpO described in Section 3. The first is the lack of an explicit definition between the solid and fluid topological domains. Depending on the value of β, the topological field will be defined as solid ($\beta = 1$), fluid ($\beta = 0$), or, more likely, slushy grey-scale β values that are neither solid or fluid ($0 < \beta < 1$). Such grey-scale regions are problematic from a manufacturing point of view, since there is no way to know where the blockage-based TopO process would choose the FSI within the grey-scale domain. Generally, the issue of β grey-scale has been treated through a cut-off approach: if β is below a certain (small) value then it is considered fluid while for larger values it is considered solidified. While convenient, this approach does not address the larger issue at hand: that the solution has not defined a true FSI. The second dilemma inherent to the blockage-based TopO formulation is the development of fluid or solid islands within otherwise homogeneous domains of the opposite type, and can be attributed to the fact that the adjoint sensitivities are applied across the entire domain. Since they have no relevance w.r.t. manufacturing, islands should not be considered when defining the FSI.

To address both these issues simultaneously, the level set (LS) method was employed as a β filter. The level set is a differential equation-driven method in which the design domains and their interfaces Γ (here Γ_{FSI}) are represented in terms of implicit functions which are monotonic and differentiable on the interface [14]. The LS method is used to manipulate its field variable ϕ, i.e. a signed distance field which must have a gradient magnitude of 1 everywhere,

$$\|\nabla \phi\| = 1 \tag{8}$$

such that $\phi_i = \{\text{negative } \forall i \in \Omega_{\text{Solid}},\ \text{zero } \forall i \in \Gamma_{\text{FSI}},\ \text{positive } \forall i \in \Omega_{\text{Fluid}}\}$

To move the FSI toward the optimal solution, the LSF is subjected to a process of convection such that the total derivative remains zero for the Lagrangian reference system. If eq. 8 holds and the convecting velocity V_i of Γ_{FSI} is defined as its unit normal multiplied by a scalar quantity, then the convection equation is derived as follows

$$\frac{\delta\phi}{\delta t} = \frac{\partial\phi}{\partial t} + \frac{\partial\phi}{\partial x_i}\frac{\partial x_i}{\partial t} = \frac{\partial\phi}{\partial t} + V_i\frac{\partial\phi}{\partial x_i} = \frac{\partial\phi}{\partial t} + V_n = 0$$

where V_n, the 'normal' convecting velocity of Γ_{FSI}. V_n is redefined as G_{Tot} and is comprised of two different contributions: those from the TopO sensitivities derived from the objective function and those from the constraint C (if imposed). The discrete form of the equation of convection is

$$\phi_m^{n+1} = \phi_m^n - (\Delta\tau)G_{Tot_m} \tag{9}$$

where

$$G_{Tot_m} = \underbrace{G_{F_m}}_{F\ Term} + \underbrace{G_{C_m}}_{C\ Term} = \frac{\delta L}{\delta\phi_m} \tag{10}$$

and $\Delta\tau$ and m are a convection step size and cell index, respectively. The F and C terms found in eq. 10 will be discussed in Section 2.4.

After eq. 9 is explicitly applied to Γ_{FSI}, eq. 8 does not necessarily hold: the ϕ field must undergo a signed-distance correction procedure (SDCorr) after each convection application. The method employed for the work in this paper corrects $\forall\phi_i \in \Gamma_{\text{FSI}}$ using the original ϕ values for those cells and then conducts a Fast Marching Method (FMM) to solve for the remainder of the ϕ domain [15]. If the computational domain is large, performing this FMM for the entire ϕ domain can be expensive. Thus, a narrow-band (NB) technique is employed in this work: the ϕ values are subject to SDCorr only if they are within the NB. Although this means that the SDCorr must be performed after each convection step (Γ_{FSI} moves and thus the NB cell set must be reassessed), the overall computational cost of the procedure becomes negligible if the NB is small.

The LS field can be trivially initialized from any given β field through the relation

$$\phi_m = 1 - 2\beta_m \tag{11}$$

which defines the zero-ϕ isoline as the FSI. Eq. 11 is an auxiliary, one-way expression: once the LSF has been convected, an inverse application of this equation will not give an accurate β field since the LS field has undergone a SDCorr and $0 < \beta < 1$ must hold (the corrected ϕ values would create β values above and below 0 and 1). Thus, after initialization the relationship between the LSF and β is inverted: β depends on ϕ according to a piecewise continuously differentiable NB sigmoidal Heavyside relationship ($\beta(\phi_m) = H(\phi_m)$). This Heavyside function differentiates into the smoothed Dirac function $D(\phi_m)$, i.e.,

$$\frac{\delta\beta(\phi_n)}{\delta\phi_m} = D(\phi_m)\delta_m^n \tag{12}$$

where δ_m^n is a Kronecker delta. This relationship is used in Section 2.4 to recast the objective function's TopO adjoint sensitivities into TopO convecting velocities.

The entire TopO process can be summarized as follows:

1. Initialize ϕ from a given β field via eq. 11.
2. Solve eqs. 1 and 6; get new field sensitivities via eq. 7.
3. Compute the LS convecting velocities G_{Tot} via eq. 10 (see Section 2.4) and convect within Γ_{FSI} via eq. 9.
4. Conduct the SDCorr process and get the new NB ϕ values based on the newly convected zero-ϕ isoline.
5. Compute $D(\phi_m)$ via eq. 12 for the next iteration's convection and set the new β field with $\beta(\phi_m) = H(\phi_m)$; return to step 2.

2.4 Level Set Convecting Velocity Term Formulation

The TopO formulation discussed in Section 2.3 requires the set of normalized convecting velocities G_{Tot} which are defined in eq. 10 and expanded as follows.

$$G_{Tot_m} = \frac{\delta L}{\delta \phi_m} = \underbrace{\frac{\partial L}{\partial \beta_n}\frac{\delta \beta_n}{\delta \phi_m}}_{F\ Term} + \underbrace{\frac{\partial L}{\partial c}\frac{\delta c}{\delta \phi_m}}_{C\ Term} \tag{13}$$

G_{Tot} is effectively comprised of two different contributions: those from the TopO adjoint sensitivities derived from the defined objective function and those from the constraint. These two contributions are discussed below and recast for the LS formulation as necessary.

Convecting Contribution G_F***: Objective Function***
Without the constraint applied, only the $F\ Term$ remains in eq. 13, which is eq. 7: the TopO sensitivities become the LS convecting velocity. To recast the TopO sensitivities as LS sensitivities, the fact that β is a function of ϕ is exploited through the relationship found in eq. 12 to give $\frac{\delta L}{\delta \phi_m} = D(\phi_m)\frac{\partial L}{\partial \beta_m}$: the TopO sensitivities are simply multiplied by the LS Dirac function. Physically, this means that the TopO sensitivities are only valid as LS convecting velocities within the NB. Thus, the $F\ Term$ in eq. 10 is

$$G_{F_m} = D(\phi_m) v_i^m u_i^m \Omega^m \beta_{MAX} \tag{14}$$

Convecting Contribution G_C***: Fluid Volume Constraint***
LS convecting velocity contributions generated from the constraint is contained within the $C\ Term$ of eq. 13. The constraint considered in this paper is an ALM equality constraint which limits the total volume-averaged sum of the β field, requiring that a certain percentage $\forbar{V}_{Fluid,Tar}$ of Ω be Ω_{Fluid}. This constraint is useful from a production perspective since limitation of the allowed fluid volume can help meet material usage restrictions. Without TopO sensitivities, only the $C\ Term$ of eq. 13 remains and is defined as

$$G_{C_m} = (-\lambda + 2wc)\frac{\delta c}{\delta \phi_m} \tag{15}$$

$$c = \frac{1}{2}(\forbar{V}_{Fluid} - \forbar{V}_{Fluid,Tar})^2, \quad \forbar{V}_{Fluid} = \frac{\int_\Omega (1 - H(\phi_m))d\Omega}{\int_\Omega d\Omega} \tag{16}$$

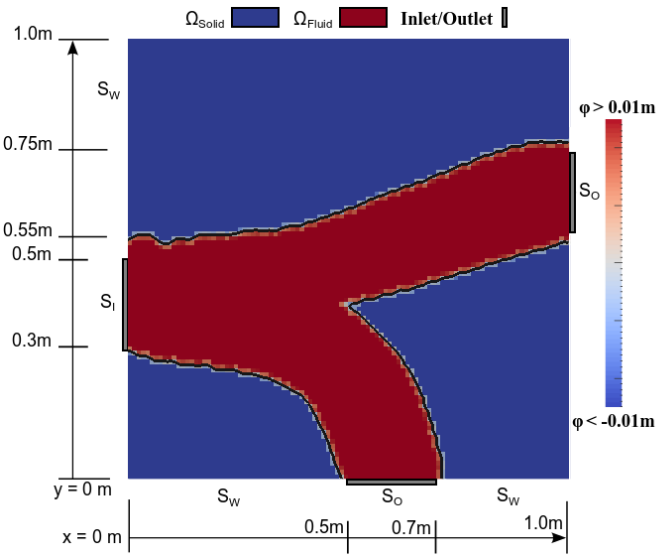

Figure 1: The TopO minimal total pressure loss ϕ solution and geometry of the TToST example case, using a NBHW of 0.01m. The Γ_{FSI} of the solution can be seen as a black line.

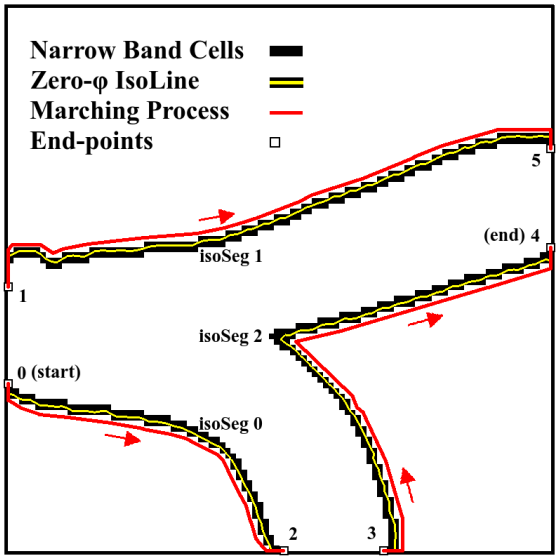

Figure 2: The marching segmentation process starts with end-point 0 and ends at end-point 4, generating points along Γ_{FSI} and assigning them to the appropriate isoPts list of each isoSeg.

3 2D TOPOLOGY-TO-SHAPE TRANSITION

The process of ShpO requires a parameterized curve or surface input in order to build a computational mesh and generate a refined, parameterized solution. In the present work, these inputs are comprised of NURBS curves. The goal of the proposed transition process is to automatically generate and fit, as closely and efficiently as possible, NURBS curves to TopO solutions so as to have a ShpO input which matches the TopO case geometry and can be fed directly into a meshing program to begin the ShpO process. This approach is only feasible due to the explicitly defined FSI found by the TopO formulation described in Section 2.3, as it provides a known target curve (the zero-ϕ isoline) to be fitted. The procedure for the proposed 2D TopO-to-ShpO transition (TToST) is explained through its application to a representative test case.

3.1 TToST Explanatory Test Case: 2D Single Inlet, Double Outlet

The case used to exemplify the TToST process is a laminar, 2D OpenFOAM (one cell in the z direction) case with one inlet to be connected to two outlets. The case has an orthogonal Cartesian mesh of 100x100 cells. β is initially specified as 0 at the cells which owned by (are adjacent to) S_I and S_O, and as 1 everywhere else. A narrow band half width (NBHW), i.e. the normal distance from Γ_{FSI} to the limits of the NB, of $0.01m$ was selected for the LS process, and the fluid volume constraint was specified with $V\!\!\!-_{Fluid,Tar} = 0.3$ (see Section 2.4). The case geometry and ϕ field solution found by the TopO process can be seen in fig. 1.

3.2 TToST Step1: Isoline Segmentation

In order to obtain a set of target curves for the NURBS fitting processes, the TopO solution's Γ_{FSI} must be decomposed into as many isoline segments (isoSegs) as there are NURBS end-point pairs to be connected. The NURBS end-points are defined at the centers of the edges

shared by boundary face pairs which have a member in both the S_W and $S_I||S_O$ face sets. The normal vectors of each point (used to define the initial, positive normal direction for a NURBS curve starting there) are defined as pointing from the S_W cell to the $S_I||S_O$ cell. For the considered case there are six end-points, requiring three isoSegs to be generated. The isoSegs are generated by interpreting an auxiliary, binary field which is 1 for cells which contain the Γ_{FSI} and 0 otherwise. During the generation process, points which lie on the zero-ϕ isoline are gathered so as to have an ordered set of points against which to fit NURBS curves in Section 3.4. The process for generating the isoSeg and their isoPts starts from an end-point and traverses the case's boundaries and Γ_{FSI} until another, unused end-point is reached, and then repeated until no end-points remain to be considered. This process is sketched in fig. 2.

3.3 TToST Step 2: ϕ Target Field Generation

The next step in the TToST is to generate a set of 'target' signed distance fields ϕ_{Tar} from each isoSeg's Γ_{FSI} cells through a SDCorr process similar to that used in the LS NB calculation (see Section 2.3). Unlike during the TopO process, the SDCorr must be performed throughout the entire domain: these target fields are used as a basis for distance comparison in step 4 of the TToST (Section 3.5) to quantify how far away from its Γ_{FSI} segment the generated NURBS is, and must therefore exist wherever the NURBS could exist within Ω. An optimization problem is solved in steps 3 and 4 of the TToST to minimize the difference between these ϕ_{Tar} fields and the NB ϕ fields generated about each NURBS curve. The use of the ϕ_{Tar} fields during this fitting process means that each NURBS curve only sees the isoSeg it is to be matched with and will not attempt to fit the other isoSegs of the case.

3.4 TToST Step 3: NURBS Least Square Fit and Parameter Search Algorithm

Once the end-points, starting normals, ordered isoPt lists and ϕ_{Tar} fields have been found, the unique initialization and fitting process for each NURBS can begin. To initiate the iterative Field Matching process described in Section 3.5 P_I points are generated on the NURBS curve, where P_I is the number of isoPts for the corresponding isoSeg to be matched, and a Least Squares Fitting problem (LSqF) is solved. The LSqF is supplied with a user-defined number of control points (nCPs) and degree which are identical for all NURBS to be fitted; 8 CPs and degree 4 for the considered example case. Performed with fixed initial nCPs and degree, the LSqF can be poor if the isoSeg has high curvature (isoSeg2) or begins away from the specified end-points (isoSeg1). A plot of the resulting NURBS curves, their CPs and the isoPts after this LSqF process can be seen in fig. 3. To mitigate the effect of these matching errors, a Parametrization Search Fit (PSF) is performed for each NURBS curve after its initialization in which the nCPs and degree are altered to decrease the error of the LSqF. The PSF algorithm set degrees 4, 3 and 2 and nCPs 9, 10 and 14 for NURBS 0, 1 and 2, respectively. A plot of the resulting NURBS curves, their CPs and the isoPts after this PSF process can be seen in fig. 4.

3.5 TToST Step 4: NURBS Field Matching Fit Algorithm

The final step in the TToST process is an iterative field comparison between a generated NURBS NB distance field, ϕ_N and the portion of its ϕ_{Tar} field within its NB which attempts to minimize $\Delta\phi_{NB}$, the aggregate difference between the two, through CP, and thus NB, displacement. Displacement for each CP is dependent on sensitivities which quantify how the current $\Delta\phi_{NB}$ relationship would change if the CP were to be moved. Thus, to properly explain the Field Matching Fit (FMF) algorithm, the formulation of its CP sensitivity generation must

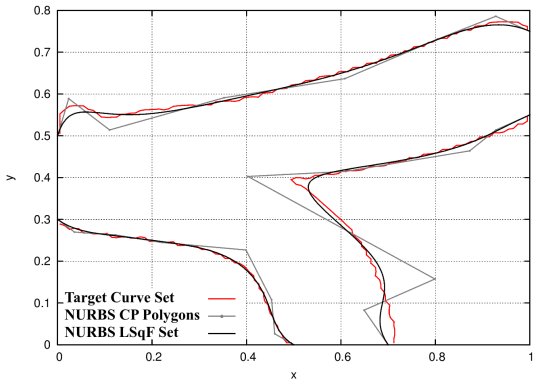

Figure 3: The TToST NURBS and their CP polygons plotted against the target TopO Γ_{FSI} solution after the LSqF process.

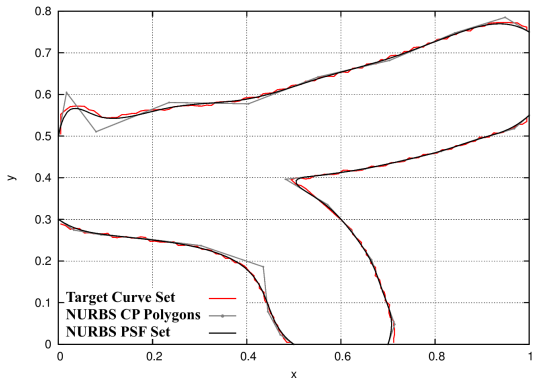

Figure 4: The TToST NURBS and their CP polygons plotted against the target TopO Γ_{FSI} solution after the PSF Algorithm.

be discussed in brief. The Field Matching (FM) objective function to be minimized and its sensitivities w.r.t. the design variables b_i are

$$F_{FM} = \frac{1}{2}\int_{\Omega} HH(\phi_N)(\phi_N - \phi_{Tar})^2 d\Omega \tag{17}$$

$$\frac{\delta F_{FM}}{\delta b_i} = \int_{\Omega} \left[\underbrace{\frac{1}{2}\frac{\partial HH(\phi_N)}{\partial \phi_N}(\phi_N - \phi_{Tar})^2}_{\Delta \mathbb{V}_{NB}\,Term} + \underbrace{HH(\phi_N)(\phi_N - \phi_{Tar})}_{\in \mathbb{V}_{NB}\,Term} \right] \frac{\delta \phi_N}{\delta b_i} d\Omega \tag{18}$$

where $HH(\phi_N)$ is a double Heavyside function which allows only the NB to be considered for integration. The $\Delta\mathbb{V}_{NB}$ term in eq. 18 describes how altering the shape of a NURBS curve through CP displacement affects a change in the NB volume, while the $\in\mathbb{V}_{NB}$ term describes the change of $\Delta\phi_{NB}$ within the current NB due the same CP displacement.

Each design variable b_i is a degree of freedom of a CP. Recast, $b_i = B_q^n$, where q is the index of the CP and n is the component of the CP which b_i pertains to. Note that both the number of degrees of freedom and the number of all components considered here is the number of dimensions of the system, D ($D=2$ for this paper). The NURBS curve has a total set of points P that can be broken into subsets P_i which pertain to the points affected by design variable b_i. Within each subset, points are denoted as p_j^k, where j is the index of the point within P_i and k is the point's component. Furthermore, each point p_j has a set $M_{i,j}$ of cells c_m within the NB which it 'owns' (i.e., which it defines the ϕ value for due to the SDCorr process), each with components denoted k due to the SDCorr relation to its curve point. Here, m is the the index of cell c within the entire NB; an index which is interchangeable with that of its ϕ value. If b_i moves, the set P_i of these NURBS points which are affected by it will also move, requiring a sensitivity relationship between b_i and $p_j \in P_i$ and between $p_j \in P_i$ and $c_m \in M_{i,j}$. The term within eq. 18 that requires this b_i to c_m coupling is $\frac{\partial \phi_N}{\partial b_i}$. If N is the set of basis functions of the NURBS defined by the parametric variable u, $\frac{\partial \phi_N}{\partial b_i}$ can be recast and found, after some derivation, to be

$$\frac{\delta \phi_N}{\delta b_i} \Longrightarrow \frac{\delta \phi_m}{\delta B_q^n} = \sum_{j=0}^{P_1-1}\sum_{k=0}^{D-1} \frac{\delta \phi_m}{\delta p_j^k}\frac{\delta p_j^k}{\delta B_q^n} = \sum_{j=0}^{P_1-1} \frac{p_l^n - c_{m(l)}^n}{\phi_m}\delta_j^l N_q(u_j) \tag{19}$$

where l is an iterate over the set P_i, subscript $m(l)$ denotes that a cell of index m is owned by the point with index l and $N_q(u_j)$ is the NURBS' derivative contribution at point u_j of the curve. The calculation of the FM CP sensitivities therefore requires a summation over all cells c_m in the NB, adding each's sensitivity contributions to all relevant CPs according to eq. 19.

The FMF algorithm, initialized with the NURBS curves found with the PSF (see Section 3.4), can now be summarized as follows for each NURBS curve to be fitted:

1. Generate points on the NURBS curve and perform the SDCorr for a defined NBHW.
2. Find F_{FM} via summation between the ϕ_N and ϕ_{Tar} fields within the NB.
3. Calculate the CP sensitivities via eq. (18) and move the CPs accordingly.
4. $IF\ |F^n_{FM} - F^{n-1}_{FM}| < \Delta F_{FM_{MIN}}, BREAK.$
5. Return to Step 1.

The FMF algorithm was run for the example case with parameters of $\Delta F_{FM_{MIN}} = 0.0001$ (a relatively high matching tolerance) and NBHW $= 0.1m$. A plot of the resulting NURBS curves, their CPs and the isoPts after the FMF process can be seen in fig. 5.

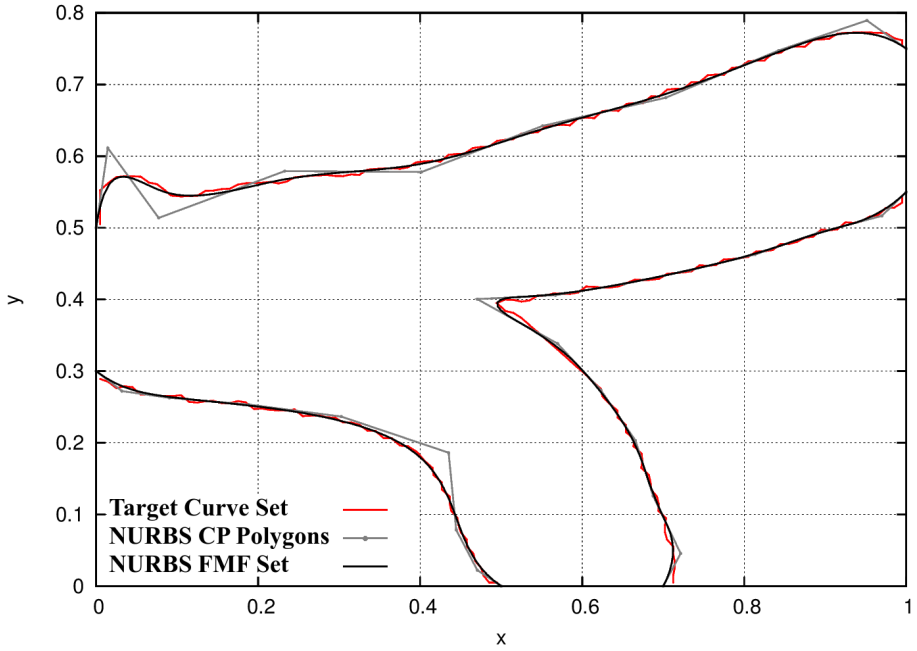

Figure 5: The TToST NURBS and their CP polygons plotted against the target TopO Γ_{FSI} solution after the FMF Algorithm.

4 SHAPE OPTIMIZATION

The TToST process (see Section 3) generates a set of NURBS curves which represent the Γ_{FSI} of the TopO solution and which can be treated as a solid wall boundary (S_W) for the primal and adjoint ShpO problem once a mesh has been generated from them. The flow equations for the ShpO are identical to eqs. 1a and 1b if the blockage term is excluded. Similarly, the

boundary conditions of the ShpO are identical to those of TopO. The design variables b_l for ShpO are, much like for the FMF optimization problem in Section 3.5, the degrees of freedom of the CPs which define S_W. The sensitivities for the ShpO CPs are computed by integrating over S_W via

$$\frac{\delta F}{\delta b_l} = -\int_{S_W} \left[\nu \left(\frac{\partial u_i}{\partial x_j} + \frac{\partial u_j}{\partial x_i} \right) n_j - q n_i \right] \frac{\partial v_i}{\partial x_k} \frac{\delta x_k}{\delta b_l} dS \tag{20}$$

where $\frac{\delta x_k}{\delta b_l}$ is computed analytically through NURBS. It is beyond the scope of this paper to present ShpO in detail; the interested reader will find material pertinent to the ShpO method and its corresponding continuous adjoint formulation in [9]. The found ShpO solution compared to the parameterized TToST NURBS solution can be seen in fig. 6. Aside from deeming the initial bulging of isoSeg1 to be insignificant on the final solution, ShpO shows preference for widening the lower and narrowing the upper exit ducts, decreasing the objective function by over 3.0% through doing so.

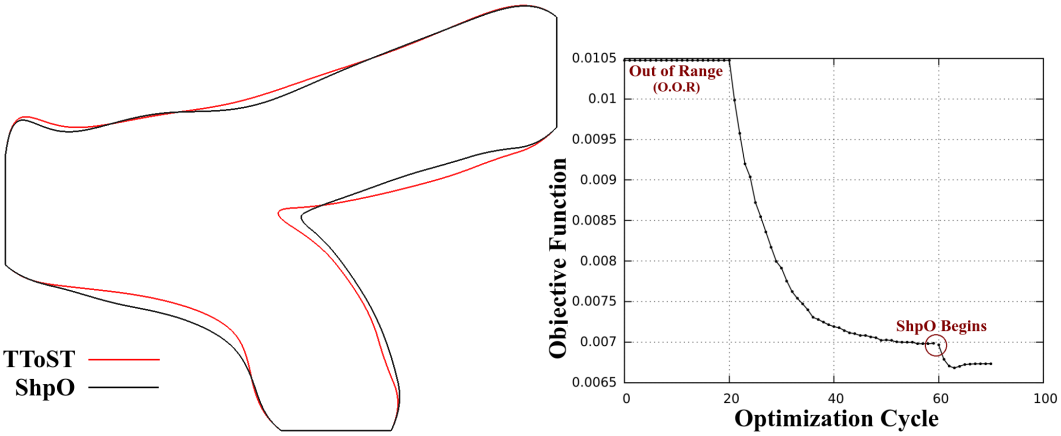

Figure 6: Example case's initial and final ShpO boundary solution (**left**) and its total pressure losses objective function's convergence history of and transitional behavior between TopO and ShpO (**right**).

The objective function trend comparison between TopO and ShpO is also shown in fig. 6. The TopO case was run to convergence to show that the continuous adjoint TopO and ShpO find similar solutions. In many applications, and as is done in Section 5, TopO would be used simply to initialize a flow channel, then let ShpO converge the solution as ShpO is considered to be faster than TopO since the zero-ϕ isoline moves only within the NB.

5 2D APPLICATION: Dual Bottle Neck Case

To demonstrate the robustness of the TToST method developed in this work, a more complex 'dualBottleNeck' case is presented. The case has a single inlet in the upper left of the case domain, two outlets in close proximity at the bottom right and two 'bottle neck' locations between them which fix the area of flow passage. The dualBottleNeck has a uniform Cartesian grid of 15200 cells and the same flow conditions, NBHW and objective function as the example case presented in Section 3. The volume constraint is similarly set to enforce $V_{Fluid,Tar} = 0.3$. The

case geometry, ϕ field solution found by the TopO process, TToST fitting solution and the final ShpO solution are shown in fig. 7.

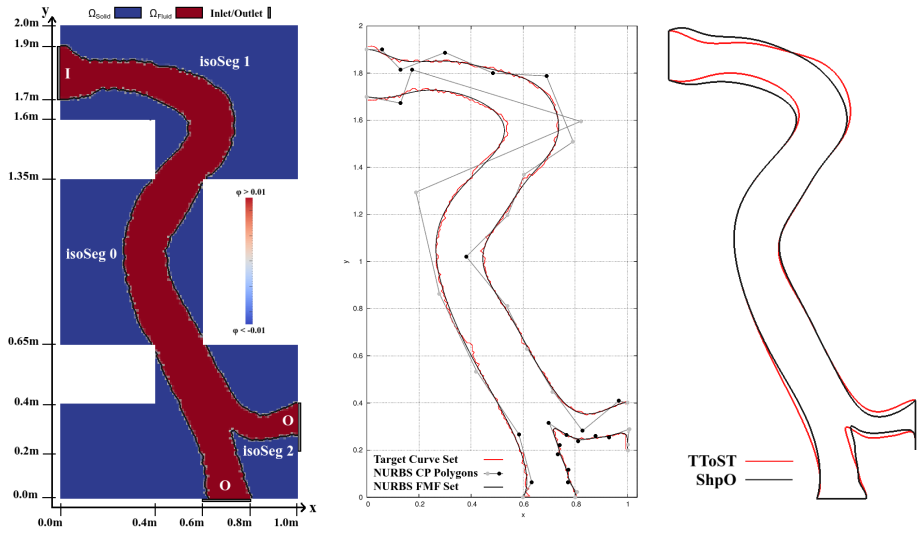

Figure 7: dualBottleNeck case solution set: (**left**): Case geometry and TopO ϕ solution with its known Γ_{FSI}. (**center**): TToST solution. Black and light grey dots indicate which control points were allowed to move and kept fixed, respectively. (**right**): The ShpO boundary solution overlaid that of the TToST.

Unlike the example case in Section 3, the dualBottleNeck case was not run to convergence during the TopO process but prematurely stopped at iteration 25 for the reasons discussed at the end of Section 4. Thus, the γ and ω ALM parameters were increased in strength to ensure the constraint be respected by the time of the TopO process' termination. Given initial degree of 4 and 10 CPs, the PSF process chose to define degrees 4, 4 and 3 and nCPs 10, 16 and 14 for NURBS curves 0,1 and 2, respectively. The FMF solution found using these parameters is shown in fig. 7, center. The two bottle necks in the case present an obstacle to the ShpO process, as its S_W boundaries are desired to remain inside the original boundary of the TopO case even though ShpO does not know where this boundary was. Thus, CPs which could affect boundary movement outside of the original TopO domain were fixed and are colored grey in the FMF solution. The ShpO process enlarges the entrance channel and carves out its lower wall in order to decrease pressure losses. It also expands the main lower exit channel. This enlarging of the lower channel was seen in the example case as well and occurs because a pressure loss is incurred when flow is diverted to the right (or upper) exit channel. Inversely, and due to the need to maintain the volume constraint, the ShpO process narrows the right exit channel.

The TopO and ShpO objective functions are plotted in fig. 8. The initial oscillation of the TopO objective is due to the severity of the imposed volume constraint since the dominance of the adjoint and constraint sensitivities can switch between iterations. A sizable objective function decrease is also seen between the end of TopO and the beginning of the ShpO: the TopO solution has not yet converged and the sensitivities are still quite large, resulting in a jagged Γ_{FSI} (see fig. 7, center) which generates pressure losses along its entire length. In contrast, all boundaries of ShpO are smooth. The ShpO process decreases the objective function by over 50%, which is not surprising due to the poor quality of the TopO's premature solution.

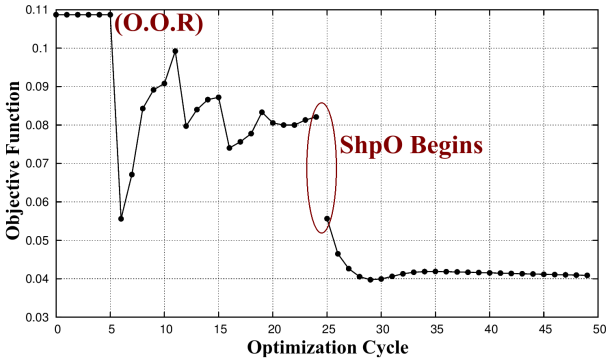

Figure 8: The convergence history of and transitional behavior between TopO and ShpO for the dualBottleNeck case's total pressure losses objective function.

6 CONCLUSIONS

The novel transitional TToST process between level-set topology and shape optimization was developed in this paper. The narrow band implementation of the continuous adjoint level set topology optimization process, TopO, ensures that the interface between the solid and fluid topological domains is explicitly defined and prevents topological island formation. Although the TopO method works well for 3D cases, its application was limited to 2D in order to showcase the TToST process, as it is currently only applicable to 2D geometries. A topological constraint for fluid volume was developed and can be used to ensure a topological solution which meets manufacturing specifications.

The 2D TToST process itself was presented, with its fitting algorithms and sensitivity calculation being discussed in detail. The cases shown in this paper demonstrate that the TToST process can accurately fit the interface defined by the TopO solution, thereby finding a parameterized NURBS set which can be used to initialize a continuous adjoint shape, ShpO, optimization problem. TToST has been shown to capture optimized solutions for both converged and pre-converged TopO problems, allowing it to decrease the overall computational cost of the linked TopO-ShpO optimization problem since ShpO's boundary movement is not limited by a narrow band like TopO. For all presented cases, ShpO allowed for a significant decrease in the objective function w.r.t. the solution found by TopO, with the improvement being more significant the sooner ShpO was allowed to take over.

Future research regarding the TToST algorithm includes expansion to 3D and the inclusion of user-defined topological islands: the current TToST algorithm would not consider floating solidified (or liquidized) islands as viable interfaces to be fitted. Validity of such an inclusion into the TToST process is under investigation.

REFERENCES

[1] M. Bendsoe and N. Kikuchi, Generating Optimal Topologies in Structural Design using a Homogenization Method. *Journal of Computer Methods in Applied Mechanics and Engineering*, **71**, 197-224, 1988.

[2] T. Borvall and J. Peterson, Topology Optimization of Fluids in Stokes Flow. *International Journal for Numerical Methods in Fluids*, **41**, 77-107, 2003.

[3] J.K. Guest and J.H. Prevost, Topology Optimization of Creeping Fluid Flows using a Darcy-Stokes Finite Element. *International Journal for Numerical Methods in Engineering*, **66**, 461-484, 2006.

[4] A. Gersborg-Hansen, O. Sigmund and R. Haber, Topology Optimization of Channel Flow Problems. *Structural and Multidisciplinary Optimization*, **30**, 181-192, 2005.

[5] O. Pironneau, *Optimal Shape Design for Elliptic Systems*. Springer-Verlag, 1984.

[6] A. Jameson, Aerodynamic Design via Control Theory. *Journal of Scientific Computing*, **3**, 233-260, 1988.

[7] W.K. Anderson and V. Venkatakrishnan, Aerodynamic Design Optimization on Unstructured Grids with a Continuous Adjoint Formulation. *Computers & Fluids*, **28**, 443-480, 1999.

[8] D.I. Papadimitriou and K.C. Giannakoglou, Aerodynamic Shape Optimization Using First and Second Order Adjoint and Direct Approaches. *Archives of Computational Methods in Engineering*, **15**, 447-488, 2008.

[9] E.M. Papoutsis-Kiachagias and K.C. Giannakoglou, Continuous Adjoint Methods for Turbulent Flows, applied to Shape and Topology Optimization: Industrial Applications. *Arch. Comput. Methods Eng.*, 1-45, 2014.

[10] S. Osher and J.A. Sethian, Fronts Propagating with Curvature Dependent Speed: Algorithms based on Hamilton-Jacobi Formulations. *Journal of Computational Physics*, **79**, 12-49, 1988.

[11] `http://www.openfoam.com`

[12] J. Nocedal and S.J. Wright, *Numerical Optimization*. Springer, 1999.

[13] E.A. Kontoleontos, E.M. Papoutsis-Kiachagias, A.S. Zymaris, D.I. Papadimitriou and K.C. Giannakoglou, Adjoint–Based Constrained Topology Optimization for Viscous Flows, Including Heat Transfer. *Engineering Optimization*, **45**, 941-961, 2013.

[14] G.K. Karpouzas and E.D. Villiers, Level-Set Based Topology Optimization using the Continuous Adjoint Method. M. Papadrakakis, M.G. Karlaftis, N.D. Lagaros (eds). *An International Conference on Engineering and Applied Sciences Optimization*, Kos Island, Greece, 4-6, June 2014.

[15] S. Osher and R. Fedkiw, *Level Set Methods and Dynamic Implicit Surfaces*. Springer, 2003.